

International Conference on Space Optics—ICSO 2022

Dubrovnik, Croatia

3–7 October 2022

Edited by Kyriaki Minoglou, Nikos Karafolas, and Bruno Cugny,



Multi-Viewing, Multi-Channel, Multi-Polarisation, Imaging (3MI) Proto Flight Model (PFM) On-Ground calibration



Multi-Viewing, Multi-Channel, Multi-Polarisation, Imaging (3MI) Proto Flight Model (PFM) On-Ground Calibration

C. Michel^a, L. Clermont^a, N. Daddi^b, F. La China^b, I. Fuentes^c, E. Mazy^a, M. Porciani^c, F. Schmutz^a, Y. Stockman^{*a}, Y. Zhao^a

^aCentre Spatial de Liège, Avenue du Pré Aily, Liege Science Park, 4031 Angleur, Belgium

^bLeonardo Spa, Airborne and Space Systems, Via delle Officine Galileo 1, 50013 Campi Bisenzio, Italy

^cESTEC – European Space Research and Technology Center, Keplerlaan 1, 2201 AZ Noordwijk, The Netherlands

ABSTRACT

The Multi-viewing, Multi-spectral, Multi-polarisation Imager (3MI) is one of the payloads that will be on board of the MetOp-SG “Satellite A”, developed to provide information on atmospheric aerosols. 3MI is a space-based, wide field-of-view polarimeter that is designed to acquire sequential images of the same ground target, which are then combined with multiple spectral views in both un-polarized and polarized channels.

This article presents the On-Ground calibration results on the 3MI PFM payload. The calibration request the measurement of a set of Key Data Parameters (KDP). These are needed in an instrument model. In the frame of 3MI calibration additionally to the geometrical, spectral and radiometric KDP, polarization and Stray Light are also considered.

Because of 3MI wide FOV and polarization performance, dedicated Ground System Equipment GSE have been developed.

Test results of the PFM calibration campaign are discussed and lessons learnt for the next campaign are proposed.

Keywords: 3MI, On-ground calibration, Earth Observation

INTRODUCTION

The baseline of the On ground calibration is to establish a relation between the output of the instrument electronic chain (Digital Number) and the physical input at the entrance on top of atmosphere (usually a spectral radiance $W/m^2.sr.nm$). This link is developed by the measurement of the main properties characterizing the instrument called KDP (Key Data Parameters). The calibration methodology is described in [2].

To measure these KDP, a set of dedicated Optical – Mechanical – Electrical and Thermal Ground System equipment (O-M-E-T GSE) have been developed and are presented in [2].

To calibrate as closed as you flight conditions, the tests are performed in a vacuum chamber with the adequate thermal environment. To not affect the thermal environment, all the source packs are placed outside the chamber and the OGSE are feed by optical fiber^[2].

The PFM calibration campaign took place between the 26/10/2021 and 31/03/2022 at CSL and the following KDP have been measured (see table here under) and will be discussed hereafter. This campaign takes advantage of lessons learnt from previous Engineering Model (EM) calibration in 2020 [2].

Radiometric tests	Spectral tests	Geometrical tests	Polarization tests	Stray light tests
Offset, Dark, Non Linearity	Out of Band	Distortion	Polarization	In FoV Spatial Point Source Transmittance (SPST)
Radiometric, Flat Field	Instrument Spectral Response Function	Line of Sight		Out Of Field SPST
		Modulation Transfer Function		

Most of the KDP are also checked in different test cases, as AIR case (not possible for the SWIR channel), in VACUUM at COLD, HOT, NOMINAL environmental thermal cases.

3MI

The goal of 3MI is to collect global observations of polarized and directional solar radiation reflected by the Earth-atmosphere system for climate and global change studies.

3MI is a complex optical instrument where sequential views of the same ground target are combined with multi-channel spectral acquisitions in both unpolarized and polarized channels. The design concept of 3MI is based on a multi-angle acquisition performed by forward, nadir and backward observations of the same on-ground target at different instants using a very wide-field optical design, a two-dimensional focal plane and use of the push-broom scanning concept in which the satellite orbital motion provides the along-track scanning [1].

The Instrument optical design consists in 2 wide Field-Of-View (114°) dioptric telescope with telecentric optics (Figure 1). The two objectives are needed to cover 2 different spectral ranges, the VNIR from 400 nm till 910 nm and the SWIR from 910 till 2130 nm. The VNIR(/SWIR) spectral range is covered by 22(/11) filters placed in a continuously rotating filter wheel. Both telescopes are aligned symmetrically with respect to the sub-satellite track (SST) materialized by an alignment cube.

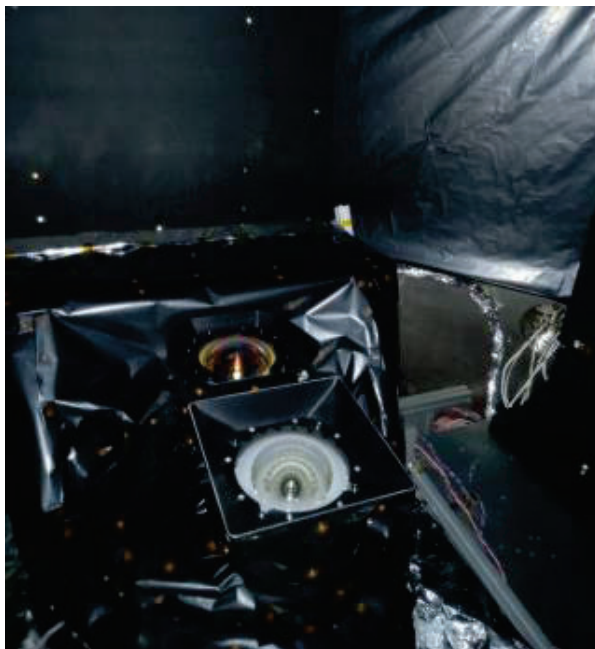


Figure 1. VNIR and SWIR camera inside the Straylight tent in FOCAL3.



Figure 2. Payload and GSE in FOCAL 3.

RADIOMETRIC CALIBRATION

The radiometric calibration addresses mainly detector properties as Offset, Dark, linearity, bad and death pixels. The conversion from DN to radiance i.e. Gain, is also part of the radiometric calibration.

Offset

The offset is the detector response when no input radiance on the system, and with integration time of 0 ms. The objective of the measurement is to determine this electronic offset and the impact of the thermal environment on it. For the offset measurement, all the light sources are off. Acquisition are performed with different integration times from ~0 ms up to 350 ms (VNIR camera) and 150 ms (SWIR camera). Since 3MI integration time is limited to 100 ms when filter wheel (FW) is rotating, the FW has been stopped for this measurement. To get a correct statistic, averaging over 100 acquisitions for each integration time is recorded. This is performed during the three thermal cases and have been repeated several times at nominal case to assess stability.

A linear regression is performed on the reconstructed signal trend vs integration time vector, see Figure 3 and Figure 4. Offset is the extrapolated signal at integration time = 0 ms.

Figure 5 and Figure 6 show the Offset computed for both cameras. The stability is about +/-0.5 DN for VNIR camera, and about +/-3.5 DN for SWIR camera. Impact of thermal case shows similar results.

The accuracy of offset measurement is mainly determined by the fitting accuracy. In VNIR, the fitting accuracy is about 0.2 DN (0.02% of VNIR offset). In SWIR, the fitting accuracy reaches 1DN (0.08% of SWIR offset). Stability over the campaign has also to be taken into account in further error budget as the other KDP measurements have been done at different times of the campaign, while only one averaged offset KDP will be used for all.

The calibration plan for offset has been well assessed in terms of environment, acquisition noise, averaging, and integration time vector. The remaining point is to correct from non-linearity (especially for SWIR detector in 3MI case) to get a correct offset KDP.

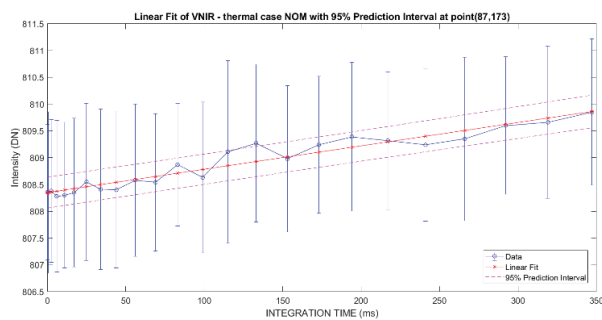


Figure 3. Example of linear regression to extract VNIR Offset KDP

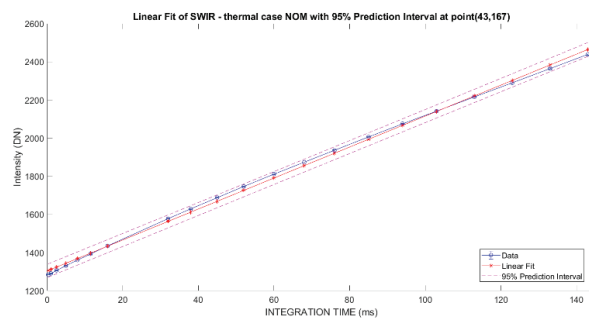


Figure 4. Example of linear regression to extract SWIR Offset KDP

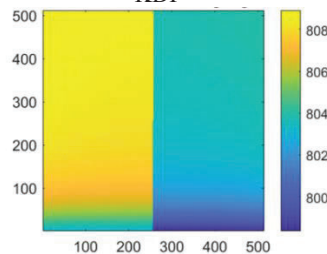


Figure 5. Offset of VNIR camera [DN].

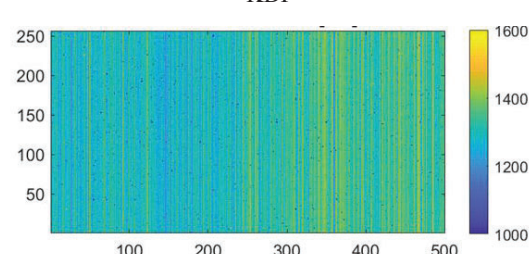


Figure 6. Offset of SWIR camera [DN].

Dark

The dark measurement consists determining the dark slope with respect to the integration time. For VNIR camera, dark slope is independent from wavelength (proved on EM). The offset measurement have then been used to extract the slope wrt integration time (see Figure 3). For SWIR camera, dark is different wrt wavelength (especially for last band at 2130 nm that can see the thermal background). The measurement has then been performed with FW rotation ON, and acquisition performed for each spectral band. Linear interpolation is then applied to get the dark slope [DN/ms].

Figure 7 and Figure 8 show the computed dark slope for both cameras. On SWIR detector, it can be observed that the Dark Slope value presents a radial trend from the detector central pixel with circular symmetry. This is due to the thermal background “footprint” detected by SWIR detector. The circular shape is due to the FPA cold shield geometrical view factor. These results are in line with outcomes from 3MI EM calibration. As for the offset, the measurements have been performed several times during the campaign to assess the stability. The different thermal cases measurement present as expected negligible impact on VNIR camera, and up to 0.5 DN/ms impact on SWIR camera.

The total accuracy of dark correction has been assessed through the correction of averaged dark acquisitions at different integration times with reconstructed dark map based on calibrated offset and dark slope. On this comparison, the accuracy of correction is about 0.22DN (VNIR camera) in worse case, with bias up to 0.5 DN. These results match the fitting accuracy and offset stability presented here above. For SWIR camera, the correction is worse, with noise up to 15DN, and bias up to 5DN for larger integration times.

Globally, the observed accuracy and stability is good. Nevertheless, SWIR detector is more tricky to calibrate, and present high sensitivity to thermal environment.

Here is then the challenge: 3MI is a wide FoV instrument, seeing all thermal vacuum chamber. Measurements need to be performed without shutter (especially for SWIR camera). The environment needs then to be perfectly dark. During calibration, some small spots on 2 filters (865 and 910 nm) have been observed. The spots came from small LEDs on displacement sensors placed on MGSE. These LEDs have been switched off as soon as it was observed.

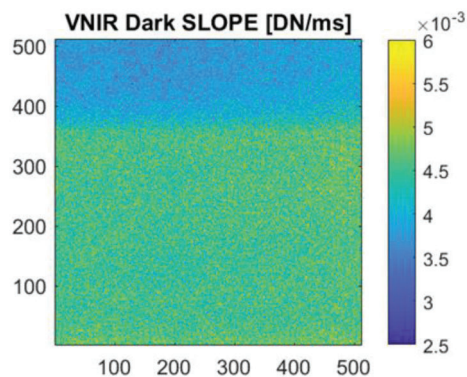


Figure 7. Dark slope on VNIR detector

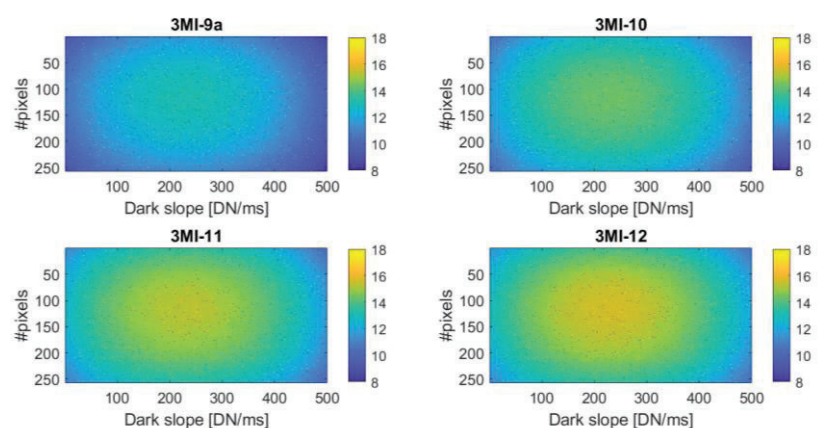


Figure 8. Dark slope on SWIR detector. 3Mi-9a = 910 nm, 3MI-10 = 1370 nm, 3MI-11 = 1650 nm, 3MI-12 = 2130 nm

Gain or absolute calibration

The KDP Gain makes the link between DN at detector level and input radiance [$\text{W}/\text{m}^2/\text{sr}/\text{nm}$]. For Gain calibration, an integrating sphere (IS) is placed in front of the instrument (see IS OGSE in [2], and picture in Figure 2), with maximum output radiance. The IS output radiance is linked to a standard through an absolute and spectral calibration performed at PTB [3], see Figure 9. This calibration has been verified both before and after calibration campaign thanks to a calibrated spectroradiometer from ESA. During Gain measurements the FW is rotating to get data for all filters. The integration time is adapted to get similar signal level on all filters (and avoid the need of non-linearity (NL) correction). These settings are the reference for Non Linearity calibration and Flat Field calibration. The light level of IS OGSE allows the use of integration times close to nominal to reach similar signal on all spectral bands, with FW rotation ON and provides a good SNR. Averaging is performed over 25 acquisitions to get an error lower than 0.1%. Measurement has been performed for three thermal cases, and several times during the campaign. The observed deviations between HOT and COLD thermal cases are lower than 0.5%.

The gain is calculated as the ratio between the signal of central pixel (after offset/dark and monitoring correction) and the reference radiance (calculated from the IS calibrated spectrum (at PTB) integrated with the measured ISRF for each spectral filter).

The Gain has been computed for all spectral bands. Results are in the expected order of magnitude wrt instrument simulations.

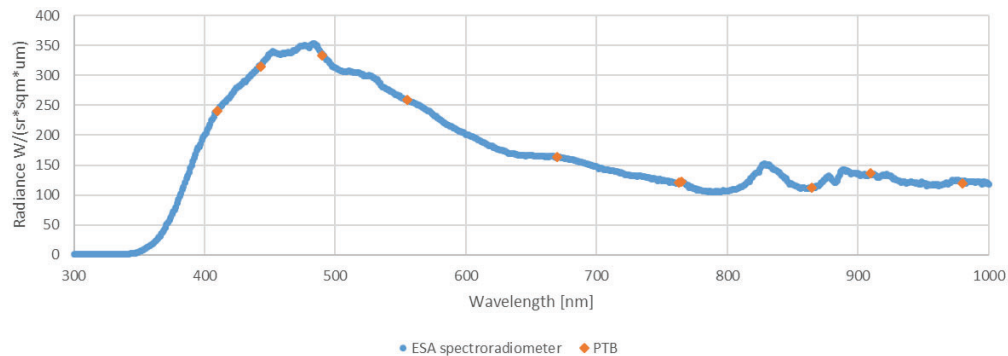


Figure 9 – IS OGSE output radiance respectively calibrated with ESA spectroradiometer (blue) and at PTB (orange).

Non-linearity

The DN conversion to radiance is not necessarily a linear function over the complete dynamic range. Determine the linearity shape and correction function is the purpose of NL measurement. Assumption is made that a variation of integration time or a variation of light level has same impact for NL behavior: the NL is only linked to the detection chain. This assumption will be verified by a test with few different light levels setup. The baseline is then to go through the full instrument dynamic with fixed input light level and integration time variation. To save testing time, only a part of the instrument FoV is measured. Consistency of detector manufacturer data was verified during EM campaign and rechecked on the sampled FOV. The detector manufacturer data will then be used to complete data over full FoV. On EM, NL was already confirmed to be independent from wavelength.

The NL is computed by comparison between effective signal, and simulation of linear behavior based on reference signal (equal to signal used for Gain KDP).

For VNIR, the measurement results match the detector manufacturer data within $< 0.2\%$ deviation (see Figure 10). For SWIR, it was also the case for EM model. Unfortunately, for current PFM model, some discrepancies are observed and are still under investigation.

Assumption that NL comes from detection chain is confirmed: there is no spectral impact, and similar results between CSL measurement and detector manufacturer measurement with completely different illumination and integration time settings are observed.

Even if detector manufacturer data validity was confirmed for EM model, measure is carried out again on PFM instrument to validate the approach.

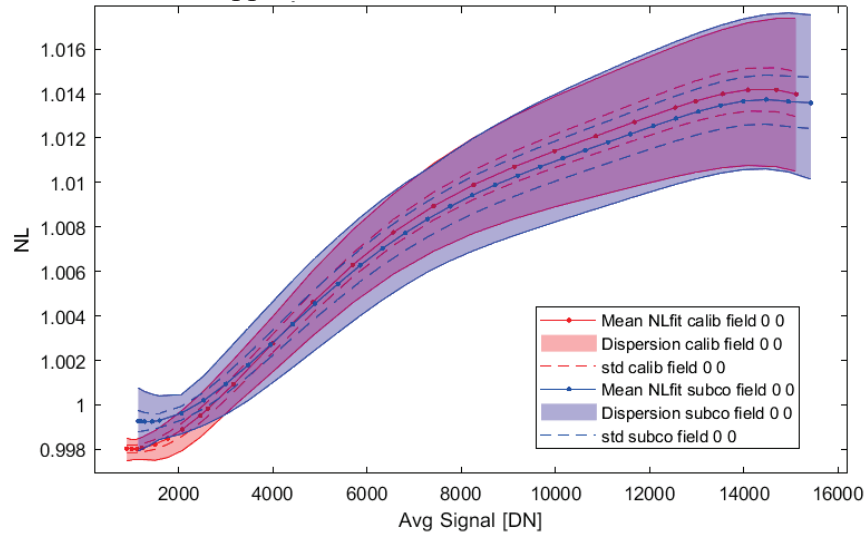


Figure 10. Comparison of detector manufacturer NL data and CSL measurements, VNIR detector.

Flat Field

The Flat Field (FF) calibration objective is to capture the pixels PRNU and instrument vignetting up to the limit of instrument FoV.

Using the IS OGSE with the same settings as for Gain calibration (maximum light level, same integration times wrt filters and FW rotating), a scanning with IS OGSE over the complete 3MI FOV is performed to provide the FF data see Figure 11. This is required since the IS OGSE illuminated only a small part of the instrument FoV (< 50*50 pixels). The distance of IS OGSE and 3MI instrument is constant, and IS OGSE always points towards the instrument pupil. To crosscheck any drift of the source additionally to the monitoring, every 15 FOV the central FOV is re-measured.

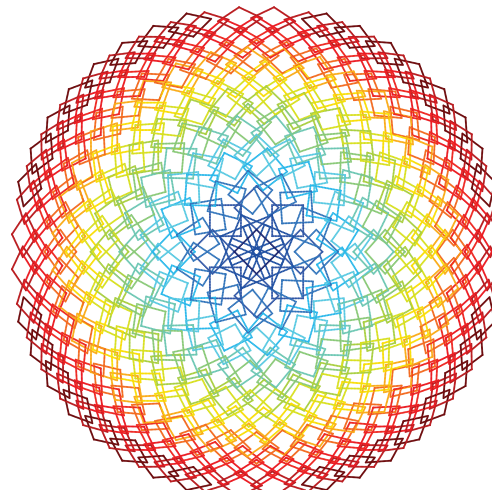


Figure 11. Scanning grid shape applied to IS displacements for FF calibration. It is a assembly of IS square footprint, organized to completely fill the input FoV of the instrument.

Each acquisition is first corrected for dark/offset. Theoretically, NL and SL correction need also to be applied. Each squared acquisition is cropped to keep only the “flat plateau” of the IS. Then the IS isotropy is corrected. The IS isotropy was calibrated prior to the campaign, with a dedicated setup. This measurement is tricky due to environment and setup stray light, not fully representative of the final configuration with 3MI instrument in front of the IS. Finally, the chosen method was to use the pattern identified on 3MI at the central FoV (PRNU removed), and remove it from all positions. Result of this subtraction is presented in Figure 12 (mainly visible for 3MI-8 765 nm filter): in central graph, a pattern composed of elongated squares can be observed, matching the sampling grid presented in Figure 11. In Figure 12, only noise remains, no pattern linked to IS is observable. In SWIR, the isotropy is also well removed, but some shapes are still present on the edges (see Figure 14): the method can still be improved. Finally, the FF is the ratio of corrected signal on each pixel wrt central pixel signal. The PRNU is obtained removing the low-frequency of the FF, as depicted in Figure 12 for VNIR. Comparison was performed wrt PRNU measured at detector level (see Figure 13). The deviation between both is below 0.34% at 1σ . For SWIR camera, the measurement at detector level highlights 4 perpendicular lines, which are not detectable on global FF measurement. The FF has been measured for all pixels, with accuracies matching the needs.

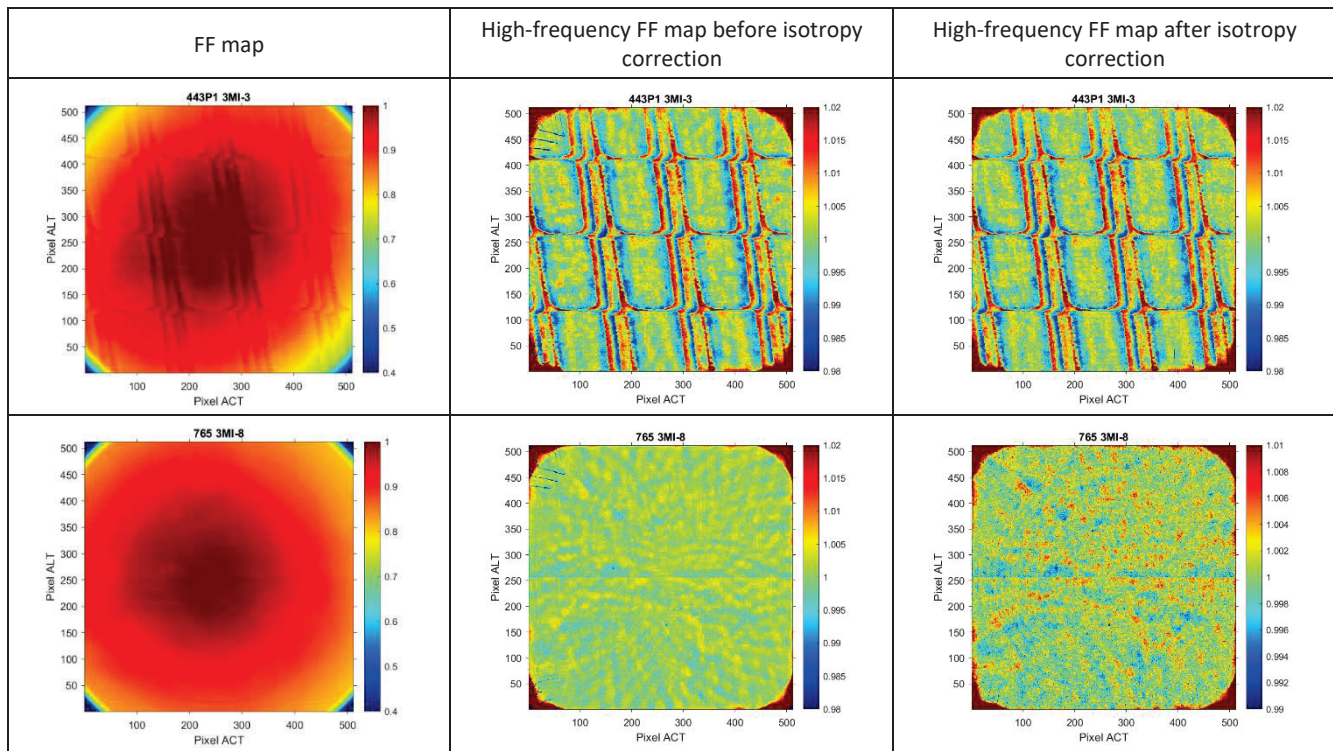


Figure 12. Comparison of the HF FF VNIR maps without isotropy correction and after isotropy correction.

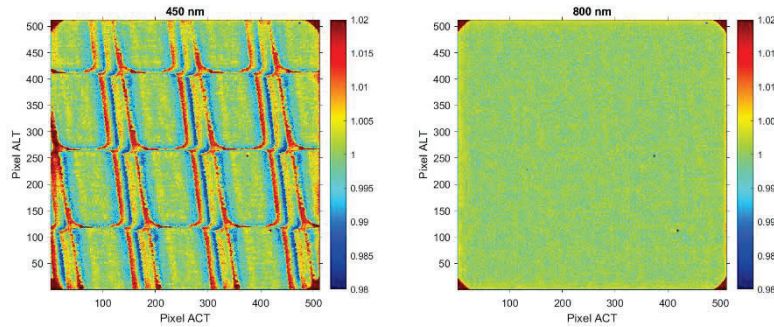


Figure 13. PRNU measured at detector level.

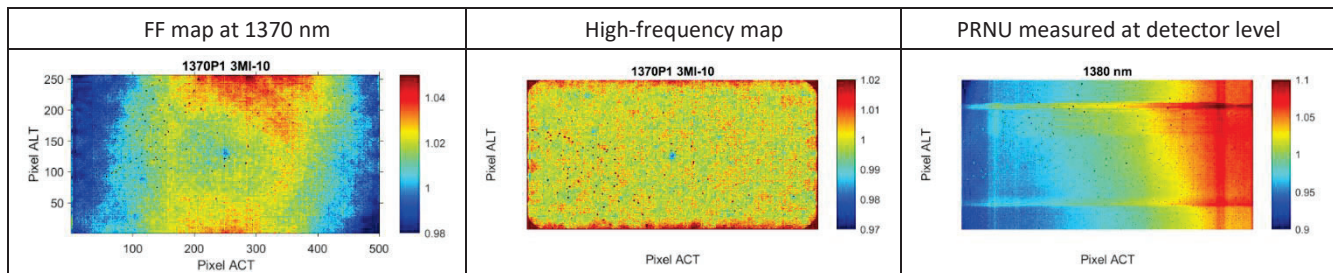


Figure 14. FF results for 1370 nm filter.

Other detector properties

Smearing

In VNIR, smearing occurs. The smearing is removed thanks to dedicated smearing lines. The correction accuracy is good ($< 0.06\%$) and might be considered negligible for non-saturated signals. However, out of the nominal conditions, the smearing behavior evolves and is no more correctable in a predicted way. It is the case during stray light calibration, where saturated signals are used. The way to account for this unexpected behaviour in the frame of stray light calibration will be detailed in dedicated paper.

Memory effect

The measurement has highlighted one unexpected features at SWIR detector level, which can be called “memory effect”. This effect gives negative print of the previous filter acquisition on the current filter (see example in Figure 15). The amplitude of this negative effect is $\sim 0.34\%$ of previous signal. After investigation, the effect was already identified by detector manufacturer. A way to remove it by post-processing is on-going for PFM, and some improvement to reduce/remove this effect on next detector generation (for FM2) is in progress at detector manufacturer level.

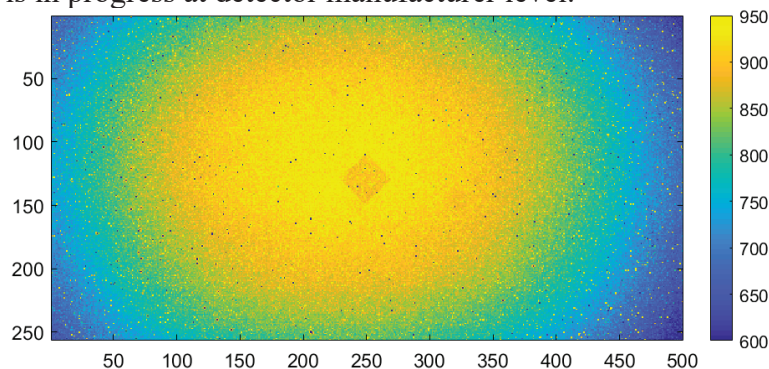


Figure 15. Memory effect on SWIR detector: IS “negative” footprint on SWIR shutter (offset removed).

SPECTRAL CALIBRATION

The goal of the spectral calibration is to characterize the ISRF (Instrument Spectral Response Function) (Figure 16) characteristics (central wavelength, channel width and spectral shape, out of band (OB)) and their behavior with respect to FOV, the optical bench temperature and integration time.

The shape of the ISRF shall be known to an accuracy of 1% of the maximum value of the ISRF for the spectral range where the ISRF is at least 1% of the maximum response.

The measurement is performed by wavelength scanning of a monochromator and by correcting the recorded signal by the monochromator spectral response.

The measurements with different integration times give a local variation much smaller than 1%; the central wavelength variation is much lower than 0.05 nm; the variation can be as low as 0.01 nm. The bandwidth variation is lower than 0.05 nm. The integration time has a negligible impact on the ISRF shape for VNIR channels. Therefore, the measurements with 100 ms integration time can be used as the final ISRF data. The stability requirement is fulfilled.

Concerning the impact of the FOV, except for the bands 3MI-2 and 3MI-9a, measurements give a local variation lower than 1% at the central part of the flat platform. However, the variation can reach 2% (6% for 3MI-7) on the border of the flat plateau. The central wavelength variation is up to 0.1 nm, and the bandwidth variation is around 0.05 nm (req~0.1 nm), except for bands 3MI-3 and 3MI-9a, which have a higher variation. The performance confirms the requirement of spatial uniformity (=1 nm).

The impact of the monochromator accuracy has also been evaluated by performing the same measurement at different times (17-05-22 and 13-08-22). The observed difference between the measurements is 0.1 nm for smaller wavelengths, up to 0.3 nm for large wavelengths. To improve the monochromator accuracy, the monochromator will be cross calibrated before each ISRF measurement by a spectral analyzer for FM2.

Similar conclusions can be drawn for the SWIR, except that the local variation is more significant, reaching 5%.

The thermal cases have a larger impact on the ISRF measurement for SWIR channels. The impact is more significant at higher elevation (40°) than at center of the FOV. At FOV center, the variation between three measurements is <0.05 for all tested bands. The variation of central wavelength is less than 0.1 nm and the variation of spectral width is less than 0.1 nm. The stability requirement is fulfilled. At FOV of 40°, the variation between the three measurements is up to 0.1 nm for all tested bands.

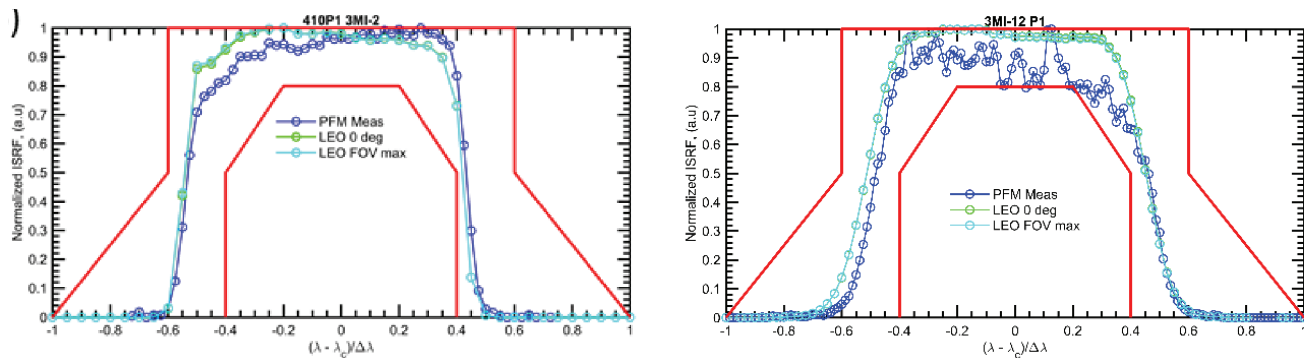


Figure 16. Example of ISRF in VNIR (Left) and SWIR (Right).

GEOMETRIC CALIBRATION

The goals of the geometric calibration are to determine the instrument distortion, Line of Sight (LoS) and to characterize its Modulation Transfer Function (MTF).

MTF

The MTF characterization has to be known versus ACT (Across Track) and ALT (ALong Track). The instrument performances is checked at Nyquist frequency.

The LSF (Line Spread Function) method is used, i.e. the MTF is computed by Fourier Transform of the LSF. To provide the LSF, the 3MI instrument is illuminated by a slit with angular divergence lower than pixel (width). The slit length covers ~ 3 pixels. The slit is scanned over 3 pixels with steps equal to $1/13$ of the current pixel angular size. Two perpendicular slits are used to get the MTF respectively ALT and ACT. 5 FoV are characterized: the central FoV, and 4 azimuths ($0^\circ/90^\circ/180^\circ/270^\circ$) with elevations used during instrument alignment.

To compute the MTF KDP, dark/offset and NL are corrected. Based on the real positioning of the MGSE with real angular step of the current scan and on real slit orientation wrt pixel orientation the LSF is reconstructed. Before applying the Fourier Transform, the LSF is deconvoluted by GSE slit size.

The iFoV is also computed based on LSF measurements for two neighbors pixels. These results are compared to iFoV based on full Line of Sight map to assess the angular step accuracy.

Figure 17 for VNIR detector and Figure 18 for SWIR detector show that the MTF results fulfills the instrument requirement. For VNIR detector, the MTF wavelength dependency is below 0.05. The azimuth symmetry shows deviations below 0.015 at Nyquist frequency. The impact of the thermal case is below 0.015 for VNIR and 0.02 for SWIR at $f/f_{nyquist} = 0.5$, fulfilling the stability requirement.

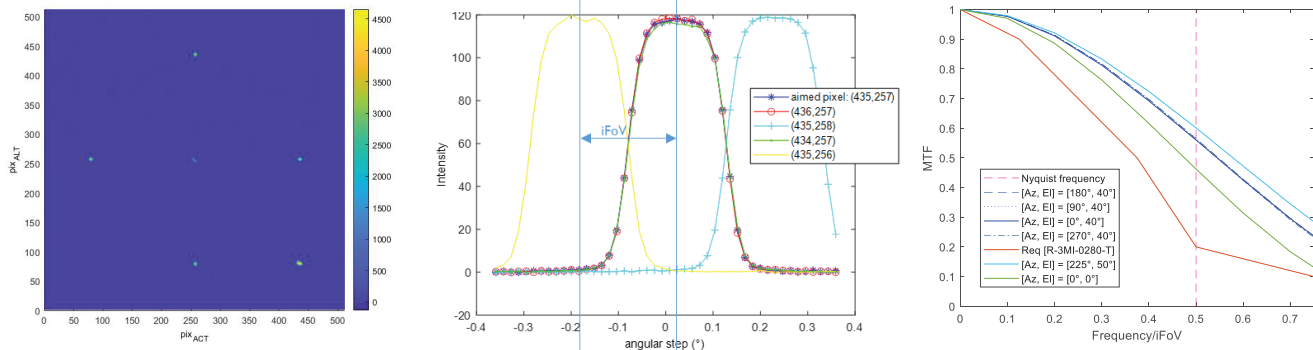


Figure 17. (left) FoV characterized on VNIR detector. (center) Example of measured LSF on three neighbors pixels. (right) Example of reconstructed MTF, compared with instrument requirement.

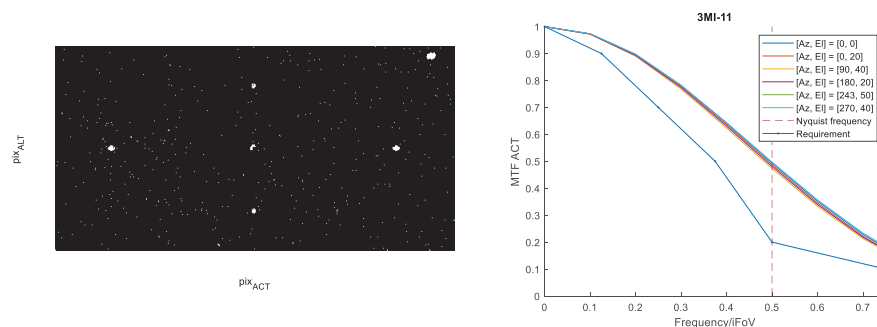


Figure 18. (left) FoV characterized on SWIR detector. (right) Example of reconstructed MTF, compared with instrument requirement.

The iFoV deviation between MTF method and Line of Sigh method is below 0.0045° . Any error in iFoV means an error on angular steps, and global error on MTF. For 0.0045° error on total angular scan, the error on MTF is about 0.007 on MTF at Nyquist. Worse case is for central FoV where MGSE accuracy is degraded: error on MTF is lower than 0.04, but for this case, as iFoV computed with LoS map is more accurate, the angular step can be adapted.

Other contributors to errors are slit size knowledge (estimated to 0.0095 based on datasheet and simulations), and acquisition noise. Acquisition SNR is over 100 for main spectral filters, but reaches $SNR = 10$ for some others. This has an impact on MTF to respectively 0.0012 and 0.012, which is still acceptable. The OGSE is diffraction limited by design. As worse case, an error of 0.018 is considered (MTF > 0.98 at Nyquist). The total accuracy (worse case) is better than 0.046 at Nyquist frequency.

Distortion

The distortion KDP will give the iFoV map, characterize the instrument distortion and provide the iLoS map, giving the Line of Sigh of each pixel wrt the 3MI instrument alignment cube reference frame.

To access the distortion map, the instrument FoV is scanned by a collimator placed on the MGSE [2]. The FoV is sampled in a way to be able to fit by a parametric surface. The used scanning grids are reported in Figure 19. These acquisitions are performed with FW rotation ON, giving the information for all the spectral bands. The integration times for each filter is adapted to get a good SNR. The spot minimum size is about 5 pixels to allow a good centroidisation computation.

The Collimator optical axis has been calibrated wrt MGSE [2] reference frame prior to 3MI calibration campaign with high accuracy. The MGSE displacement is referenced in 3MI alignment cube reference frame at AIR. The absolute displacement of the MGSE is computed based on a set of transfer matrices related to each rotating element, and calibrated correction layers (including MGSE frame deformation wrt moving stage position, wobble, ...). A final calibration with laser tracker is planned to assess the real positioning with accuracy better than 20 arcsec.

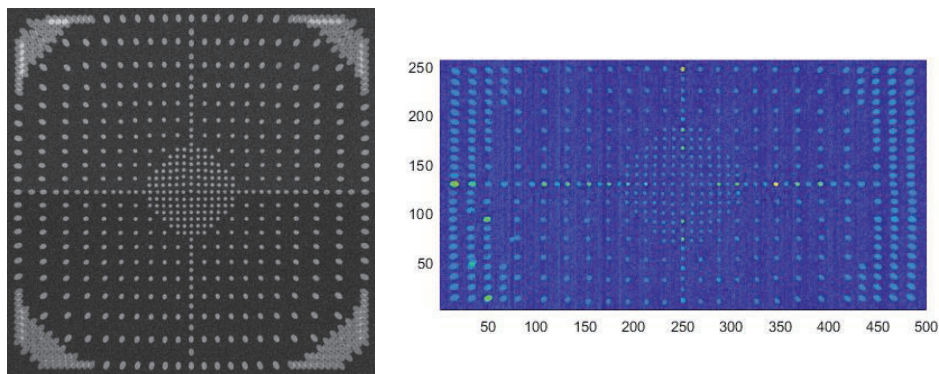


Figure 19. Scanning grid for iLoS map calibration, respectively on (left) VNIR detector and (right) SWIR detector.

As for most of the KDP computation, the spot is corrected from dark/offset and FF. The Centrodization is performed to get the central pixel coordinates, in relation with known input [Azimuth, Elevation] position. The central pixel corresponding to MGSE rotation center is identified. The map is then centered on this pixel. The obtained map is fitted in two steps: first with theoretical $f \cdot \tan(\theta)$ function, for elevations $< 30^\circ$, to get the focal length and pixel size, then, with a dedicated function over the full FoV based on Brown's distortion model:

$$\begin{aligned}x_d &= f \cdot \tan(\theta_x); \\y_d &= f \cdot \tan(\theta_y);\end{aligned}$$

$$r = \sqrt{x_d^2 + y_d^2}$$

$$Eqn_X = f.tand(x) + x_d.(k_1.r^2 + k_2.r^4 + k_3.r^6 + k_4.r^8) + (p_1.(r^2 + 2.x_d^2) + 2.p_2.x_d.y_d).(1 + p_3.r^2 + p_4.r^4 + p_5.r^6 + p_6.r^8)$$

$$Eqn_Y = f.tand(y) + y_d.(k_1.r^2 + k_2.r^4 + k_3.r^6 + k_4.r^8) + (2.p_1.x_d.y_d + p_2.(r^2 + 2.y_d^2)).(1 + p_3.r^2 + p_4.r^4 + p_5.r^6 + p_6.r^8)$$

$$Eqn = \frac{1}{D} * \sqrt{Eqn_X^2 + Eqn_Y^2};$$

To get absolute positioning, LOS OGSE results are used to apply angular correction, see next section. Finally, iFoV map is computed as the cosinus of scalar product between to neighbors pixels LoS vector. The analysis of the central part fitting has allowed the identification with high accuracy of a constant offset in MGSE elevation. This was already identified during laser tracker check before calibration campaign. This offset has been applied for all further positions. The Central part was fitted with accuracy better than 0.1 pixel PtV (both VNIR and SWIR detectors). Results of focal length (Figure 20) and pixel size are consistent with theoretical model. The distortion is below requirement, and matches also the theory (Figure 21). The iFoV map is computed (Figure 22), with results consistent wrt iFoV obtained during MTF calibration. Same conclusion can be drawn for SWIR.

The iLoS map was fitted over full FoV. Deviations between fitted surface and measured points are plotted in Figure 23: standard deviation is below 0.02° (VNIR) and 0.008° (SWIR) over full FoV, but systematic deviation are observed. These deviations are expected to come from MGSE inaccuracies. A full calibration of MGSE to improve results is on-going. The pixel size is 0.27° at central FoV, the map accuracy is then quite good (better than 1/10 of pixel), even if not yet fully compliant with requirement (asking for 3/100 of pixel).

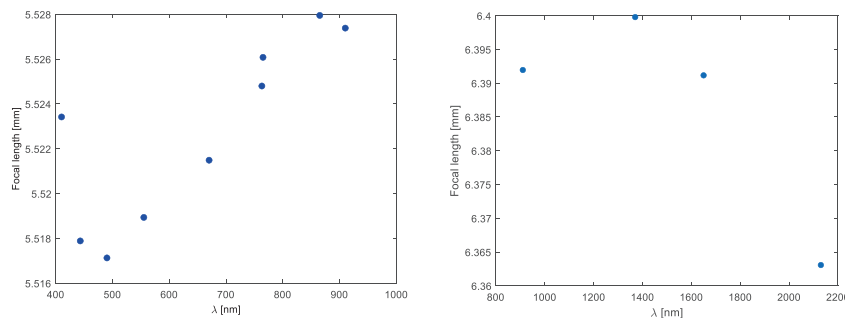


Figure 20. Focal length wrt wavelength respectively for (left) VNIR detector and (right) SWIR detector.

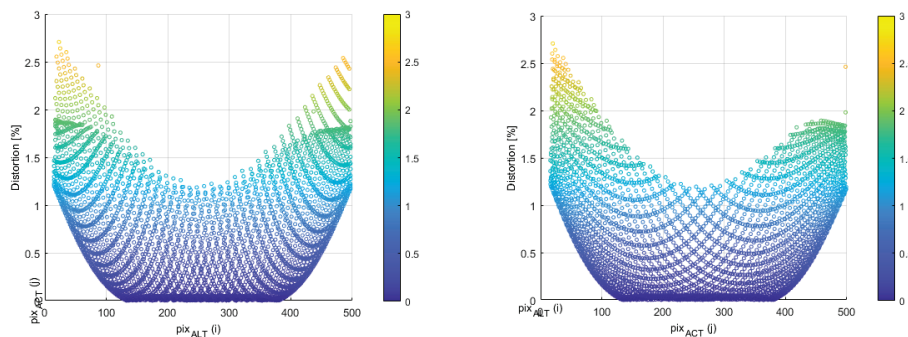


Figure 21. Distortion map for VNIR detector.

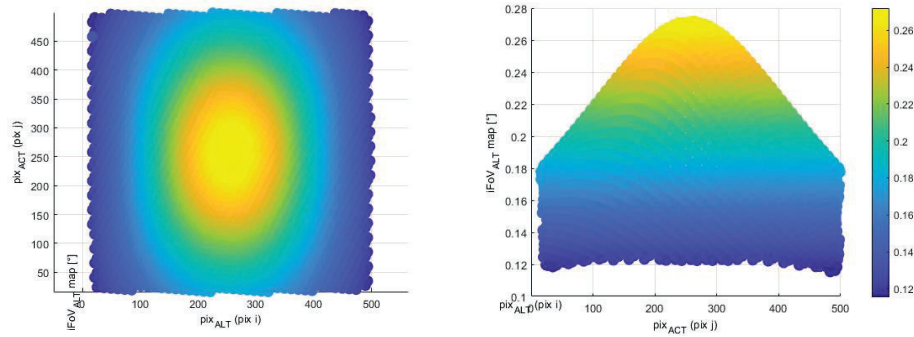


Figure 22. iFoV map along ALT direction. VNIR detector.

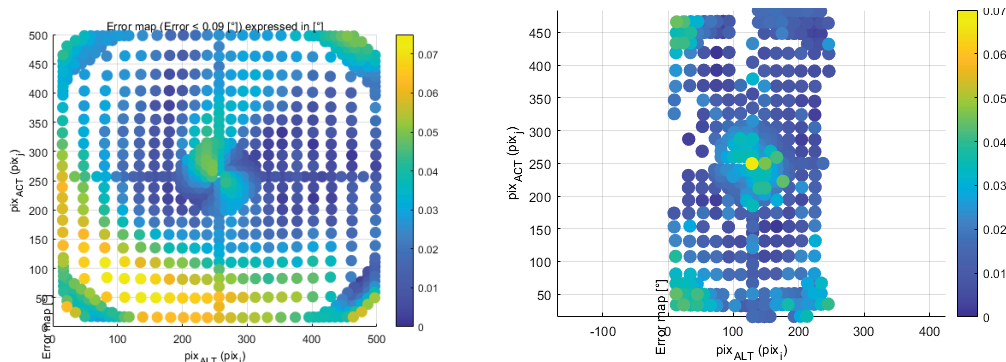


Figure 23. Fitted map error, respectively for (left) VNIR camera and (right) SWIR camera.

Line of Sight

The MGSE used for iLoS map calibration is referenced wrt instrument alignment cube at AIR. However, the cube (and 3MI interface) might slightly moves when going under vacuum or changing the thermal environment. To monitor the cube displacement, a dedicated GSE has been implemented on the upper structure of the MGSE [2]. The stability of this GSE when going under vacuum has been tested and validated during blank test prior to the calibration campaign. The LOS GSE monitor the alignment cube orientation, and send parallel beams on both VNIR and SWIR camera. Measurement of corresponding spots on both camera is performed with FW rotation ON, so for all filters, with adapted integration times to get enough signal. The measurement is repeated locally to get some statistics, and is also repeated at each thermal phase. The Line of Sight pixel coordinates on both camera correspond to the center of the illuminated spot, with angular correction corresponding to the cube deviation wrt reference position.

This monitoring measurement was very useful in the sense that it identified a solid displacement of about 90 arcsec on alignment cube and both camera wrt LOS OGSE between the thermal cases and between Air and Vacuum environment. Without this monitoring GSE, it could not be possible to discriminate between camera displacement wrt 3MI interface, or global 3MI interface displacement.

The global displacement is assigned to the feet of the interface on which 3MI is fixed. These feet experienced some thermal gradient that, if not perfectly symmetrical between all feet, can explain a tilt. The iLoS map measured with MGSE (see previous section) is then adjusted such as elevation = 0° coordinates corresponds to the pixel identified as parallel to alignment cube by LOS GSE. Applying this correction, the stability between both VNIR and SWIR camera is measured to be better than 0.05 pixels, which is fully compliant with the requirement.

The achieved accuracy on coordinates for both VNIR and SWIR camera is computed to be below 12 arcsec. This error includes: OGSE cube/VNIR/SWIR beams co-alignment, centrodization on 3MI

cameras, characterization of cube orientation wrt reference point, iFoV accuracy for corresponding displacement on 3MI detectors.

Even if this specific GSE is not expressly required (the MGSE referenced wrt alignment cube in air shall be enough), this implementation was a good point, since it allows the identification of unexpected interface deviation, and its correction, leading to good conclusions regarding instrument stability that might be non-compliant if only MGSE was used.

POLARIMETRIC CALIBRATION

Because 3MI is a polarimetric instrument, the polarization calibration is a major KDP to calibrate. The aim is to determine the Mueller matrices corresponding to each filter, and for each pixel.

Since the 3MI polarization sensitivity evolves with FoV, a grid of points to calibrate has been established based on simulations in order to be able to fit the results over full FoV. The sensitivity wrt FOV and the grid are presented in Figure 24 for VNIR camera.

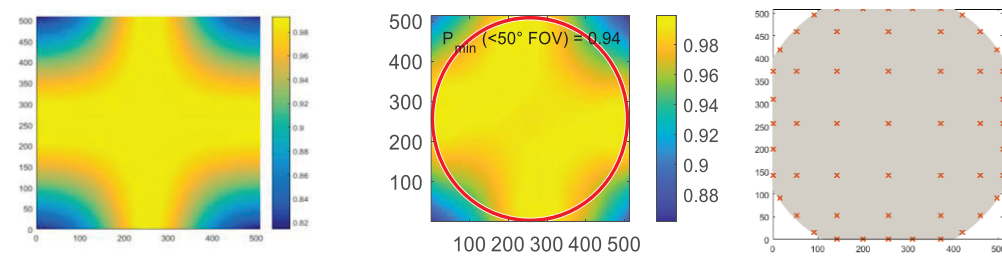


Figure 24. Theoretical (left) and measured (center) sensitivity map for polarized filter at 490 nm. (right) Grid for polarization calibration – VNIR camera.

The GSE used for this calibration is a collimator illuminating ~ 5 pixels, with a rotating linear polarizer in front of the output [2]. The polarizer extinction ratio is $> 10000:1$, to not limit the calibration accuracy. The polarizer is rotated from 0° up to 360° with 4° steps. As the filters of 3MI are rotating, their sensitivity evolves also according integration time. Calibration wrt integration time is also performed. The final objective is to find a fitting model for the integration impact on the Mueller matrices.

The measurement is performed by illuminating each pixel, and recording the signal versus the GSE polarizer orientation. Of course the signal is corrected by dark/offset and NL, and GSE. Additionally the polarizer angular position is corrected according absolute calibration performed prior to calibration campaign. The corrected signals and angular vectors are then fitted by a Malus law, see example in Figure 25. To complete the computation a FoV fitting and respectively an integration time fitting are performed.

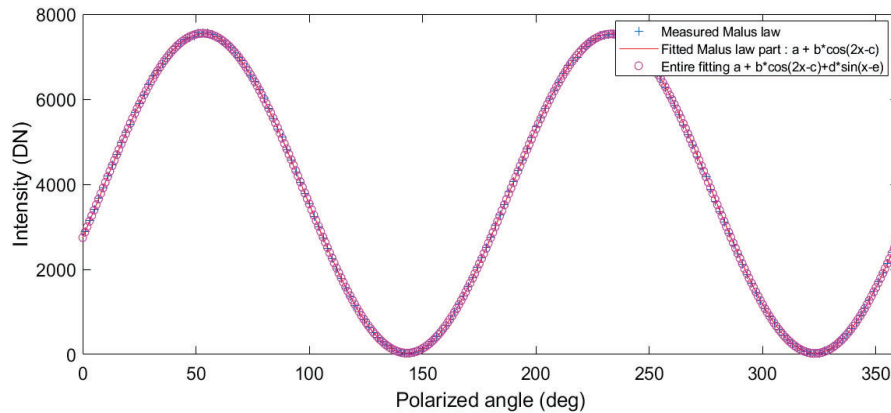


Figure 25. Example of Malus law fitting.

The filters sensitivity has been calibrated for all FOV planned. The resulting sensitivity map shape is consistent with theory, with lower amplitude variation wrt FOV than expected, which is a good news (see Figure 24). The accuracy for large wavelength is better than 0.001, which matches the requirement. Relative and absolute angle of polarization is also consistent with expectation..

STRAY LIGHT CALIBRATION

A full calibration campaign of stray light has been performed on both VNIR and SWIR camera. The measurements cover all spectral bands, and some additional tests to investigate the impact of polarization. Results will be detailed in a dedicated coming paper. Principle used for calibration and correction of stray light are detailed in references [4][5][6].

CONCLUSIONS

3MI instrument calibration is a wide and long calibration campaign. Its wide FoV and the need to look up induces large constraints on both MGSE and facility stray light. The polarization properties are always challenging, and stray light calibration is very demanding, leading to different optimizations and light sources modification during the campaign. The total duration is more than 80 days under vacuum. To cover all tests in a more efficient way, all GSE and 3MI acquisition sequences related to each KDP have been successfully automatized.

The calibration campaign has been performed in agreement with calibration plan. All issues encountered during the campaign (at MGSE, GSE, lasers, ...) levels have been overcome, and at the end, all required data have been acquired, successfully checked during the campaign, and finally classified with all information.

Globally, all computed performances of PFM are in the range of expected values, but fine analysis highlights some difficulties or unexpected behaviors. Part of them have been solved thanks to redundant measurements performed during the campaign. Other are still under investigation.

ACKNOWLEDGMENTS

The work is performed under ESA contract 4500511744/MetOp-SG/CSL between Leonardo and Centre Spatial de Liège.

The authors are grateful to all the CSL operators that spend day and night, weekends included to acquire correctly all the data and to face and correct all the unexpected problems, as well to Leonardo operators for they support on the payload operations.

Great thanks to Angelos Giannopoulos for its support to solve in real time all the MMI (Master Computer) issues.

REFERENCES

- [1] Manolis, Al, "The 3MI instrument on the METOP second generation", International Conference in Space Optics ICSO (2014).
- [2] C. Michel, Al "3Multi-Viewing, Multi-Channel, Multi-Polarisation Imaging (3MI) Engineering Model (EM) On-ground calibration" SPIE Astronomy and telescope instrumentation, Montreal 2022
- [3] PTB calibration report 73110 PTB21, Berlin 2021
- [4] Clermont, Al, "The stray light entrance pupil: an efficient tool for stray light characterization" Optical Engineering 191528 (2020)
- [5] Clermont, Al, "Post-processing correction of stray-light in space instruments: application to the 3MI Earth observation instrument" International Conference in Space Optics ICSO 2018
- [6] Clermont, Al, "Out-of-field stray light correction in space telescopes: the case of Metop-3MI", SPIE ASTRONOMY 2022